Article

Discovery Medicine 2025; 37(192): 166–181
https://doi.org/10.24976/Discov.Med.202537192.14

Glioblastoma Stem Cells: MAP17 as a Novel Predictive Biomarker and Therapeutic Target Associated with Quiescence and Immune Evasion

Sara Sadat Aghamiri[1], Rada Amin[1,*]

[1]Department of Biochemistry, University of Nebraska, Lincoln, NE 68503, USA
*Correspondence: raminali2@unl.edu (Rada Amin)
Published: 20 January 2025

Background: Glioblastoma multiforme (GBM) is one of the deadliest and most heterogeneous forms of brain cancer, characterized by its resistance to conventional therapies. Within GBM, a subpopulation of slow-cycling cells, often linked to quiescence and stemness, plays a crucial role in treatment resistance and tumor recurrence. This study aimed to identify novel biomarkers associated with these slow-cycling GBM cells.

Methods: We utilized The Cancer Genome Atlas (TCGA)-GBM dataset and presented the reproducible bioinformatics analysis for our results.

Results: Our analysis highlighted Membrane-Associated Protein 17 (*MAP17*) as strongly associated with the slow-cycling phenotype. We found that the protein cargo *MAP17* expression is related to mesenchymal signatures and stem cell-related pathways. Also, *MAP17* was linked to a distinct metabolic profile, characterized by significant enrichment in pathways related to folate, zinc, and fatty acids. Moreover, the immune cell distribution analysis revealed that *MAP17* correlates with key molecular immune processes, including interferon-gamma (*IFN-*γ) signaling and antigen presentation, as well as immunosuppressive cells like myeloid-derived suppressor cells (MDSCs) and macrophages. *MAP17*-high tumors also showed elevated expression of several immune checkpoint inhibitors, indicating an immunosuppressive microenvironment.

Conclusion: These findings provide insight into the role of *MAP17* in quiescence, stemness, and immune evasion, positioning it as a promising therapeutic target.

Keywords: glioblastoma; slow-cycling cells; mesenchymal; immune cells; biomarkers; cancer stem cells

Introduction

Glioblastoma multiforme (GBM) is a treatment-resistant brain tumor, primarily due to its molecular and phenotypic heterogeneity. This heterogeneity arises from several factors, including clonal evolution, spatial variability within the tumor, and the selective pressures exerted by therapeutic interventions [1]. The therapeutic resistance and intratumoral heterogeneity are caused by the presence of a subpopulation of cancer stem cells (CSCs), which play a key role in re-establishing aggressive and therapy-resistant clones. CSCs contribute to tumor resilience, recurrence, and metastasis due to their self-renewal capacity, quiescence, and phenotypic plasticity [2]. GBM stem cells (GSCs) exhibit active DNA repair mechanisms, leading to recovery from the damage caused by radiation and chemotherapy [3]. Intriguingly, the GSC population consists of diverse microstates and subclones that can persist within the same tumor. This diversity is influenced by the tumor environment (TME) and therapeutic interventions. For instance, two primary stemness subtypes have been identified: proneural GBM stem cells (PN-GSCs) and mesenchymal GBM stem cells (MES-GSCs), which have been shown to transition from PN to MES to acquire more resistance and invasive properties [4]. Furthermore, GSCs also exhibit a hierarchical structure based on cycling dynamics and metabolic activity, categorized into fast-cycling cells (FCCs) and slow-cycling cells (SCCs). SCCs, often quiescent, are known to expand with more resistance properties, indicating their critical role in driving therapy resistance and tumor recurrence [5]. In an *in vivo* model of chemotherapy-resistant GBM, SCCs promote tumor growth by generating fast-growing clones that are closely associated with chemoresistance [6]. To distinguish FCCs from SCCs, various markers have been proposed, including the proliferation marker KI67, transcription factors, signaling kinases, epigenetic regulators, metabolic modulators, and surface markers [7–9]. The plasticity of GSCs complicates the establishment of a definitive marker panel. As a result, biomarkers that are relevant during the early stages of tumorigenesis may lose their applicability as the disease advances and metastasizes [10].

The malignancy of GSC is further sustained by a complex interplay between tumor cells and neighboring cells,

which collectively form specialized niches within TME. The ecosystem plays a pivotal role in regulating stemness, survival, metabolic adaptation, immune evasion, and therapy resistance. Mechanisms contributing to these functions include altered extracellular matrix (ECM) organization, the formation of hypoxic niches, and the development of dense vasculature, all of which impede effective therapy and drug delivery to tumor sites [11]. GSCs employ diverse mechanisms of immune evasion, including the recruitment of immunosuppressive immune cells such as regulatory T cells (Tregs) and myeloid-derived suppressor cells (MDSCs), the secretion of immunosuppressive cytokines, the upregulation of immune checkpoint molecules, and impairments in immune recognition due to defective antigen presentation by antigen-presenting cells (APCs). These strategies collectively contribute to immune escape, fostering an environment that protects GSCs, and limits the success of immune-based therapies [12,13]. For instance, immune checkpoint inhibitors (ICIs) targeting programmed death-ligand 1 (PD-L1), programmed cell death protein 1 (PD-1) (e.g., pembrolizumab, nivolumab), or cytotoxic T-lymphocyte-associated protein 4 (CTLA-4) (e.g., ipilimumab) have shown success in various cancers by restoring T cell activity. However, their efficacy has been markedly limited in GBM [14,15]. This is largely due to the dominance of immunosuppressive cells, the poor infiltration of effector T cells, and niche heterogeneity [16]. Altogether, the intratumoral diversity at the molecular and cellular scale within CSCs and TME highlights the complexity of GBM and the challenges in developing effective treatments. Identifying novel biomarkers that address GBM heterogeneity will be pivotal in guiding personalized interventions to overcome resistance and recurrence.

In this study, we aimed to identify novel markers that can specifically define the SCCs in GBM. To achieve this, we first stratified The Cancer Genome Atlas (TCGA)-GBM cohort based on the marker of proliferation KI67 (*MKI67*) gene expression (gene encoding for the protein KI67) and analyzed the differential gene expression associated with low *MKI67*. This approach led us to identify Membrane-Associated Protein 17 (*MAP17*) as a potential novel biomarker for defining SCCs. MAP17 demonstrated both clinical and histopathological significance in GBM. Furthermore, differential gene analysis revealed that *MAP17* is associated with a stemness phenotype, immune processes, and an immunosuppressive microenvironment.

Materials and Methods

Clinicopathological Correlation and Enrichment Analysis Based on Xena Analysis

The University of California-Santa Cruz (UCSC) Xena database [17] (https://xena.ucsc.edu/) is an interactive tool for multi-omics, clinical, and phenotype data analysis. Xena provides 154 cohorts from various sources such as TCGA, and genomic data commons (GDC), as well as other genomic data including microarray, copy number alterations, somatic mutations, and DNA methylation data. The cohort used for the present study is RNA-sequencing (Illumina HiSeq) TCGA-GBM with 172 samples. This dataset shows the gene-level transcription as in Log2 (norm count+1), in which the norm count refers to RNA-Seq by Expectation Maximization (RSEM) value. The TCGA-GBM cohort (n = 172) was stratified into two groups based on the median *MKI67* gene expression for each dataset. The low *MKI67* groups expressed Log2 (norm count+1) <9.64, while the high group presented Log2 (norm count+1) >9.64. We identify canonical pathways that were differentially expressed between the *MKI67* high and low-expression groups using the gene set enrichment analysis (GSEA) from the module "GSEA" available in the Xena analysis tool. The cut-off criteria for differentially expressed genes (DEG) selection (differentially expressed genes) was as follows: $|\log2\text{-fold change}| > 1.5$, $p < 0.05$, and false discovery rate (FDR) <0.05. We represented the top pathways with significant enrichment in either upregulated or downregulated *MKI67* groups, based on an adjusted *p*-value (adj-P) of <0.0001, which considered significant. To evaluate the significant gene associated with SCCs within the *MKI67*-low group, we selected the gene based on the threshold of log fold change (logFC) threshold of <-1.5 and a *p*-value $<$ 0.0001 and found 24 genes based on these criteria. The 24 genes, arranged alphabetically, are: Chromosome 6 Open Reading Frame 15 (*C6orf15*), Cholecystokinin (*CCK*), CD3 Delta Subunit (*CD3D*), Chitinase-3-Like Protein 1 (*CHI3L1*), Chitinase-3-Like Protein 2 (*CHI3L2*), Chondrolectin (*CHODL*), Cytochrome P450 Family 11 Subfamily A Member 1 (*CYP11A1*), C-X-C Motif Chemokine Ligand 5 (*CXCL5*), Family With Sequence Similarity 183 Member A (*FAM183A*), Haptoglobin (*HP*), Interleukin 20 Receptor Subunit Alpha (*IL20RA*), Leucine-Rich Repeat-Containing G Protein-Coupled Receptor 6 (*LGR6*), Lipase C (*LIPC*, Hepatic Type), Lactotransferrin (*LTF*), Membrane-Associated Protein 17 (*MAP17*), Myosin Binding Protein C1 (*MYBPC1*), Otospiralin (*OTOS*), Peptidase Inhibitor 3 (*PI3*), Phospholipase A2 Group V (*PLA2G5*), Phospholipase A2 Group IIA (*PLA2G2A*), Serum Amyloid A1 (*SAA1*), Serum Amyloid A2 (*SAA2*), Secretory Leukocyte Peptidase Inhibitor (*SLPI*), and Solute Carrier Family 39 Member 12 (*SLC39A12*).

The overall survival (OS), disease-specific survival (DSS), and progression-free interval (PFI) data were extracted for the 24-gene set from the *MKI67*-low groups and visualized as a heatmap showing the -log10 rank test *p*-values for each gene. We compared OS, DSS, and PFI between high- (Log2 (norm count+1) >4.28) and low-*MAP17* risk groups (Log2 (norm count+1) <4.28), using the median value as the cutoff. The analysis was performed using Kaplan-Meier survival curves, and statistical signifi-

cance was assessed with the log-rank test (**Supplementary Fig. 1A**). The normalized gene expression of *MAP17* in different subtypes was also extracted from the same cohort. After selecting *MAP17* as the primary candidate for further investigation, we conducted a similar GSEA analysis based on the same median expression of *MAP17* comparing high versus low groups, evaluating Hallmark, Reactome, Biocarta, GBM subtypes-related pathways (classical, proneural, and mesenchymal), and metabolic- and stemness-related pathways. To assess the cycling status of *MAP17*, we analyzed the expression of fast-cycling genes (cyclin-dependent kinase 2 (*CDK2*) [18], and cyclin B1 (*CCNB1*)) and slow-cycling genes (cyclin-dependent kinase inhibitor 1A (*CDKN1A*) and G0/G1 switch gene 2 (*G0S2*)), reporting the Spearman correlation coefficients and *p*-values [19].

To assess the correlation between *MAP17* expression and PN-GSCs and MES-GSCs phenotypes, we utilized gene sets from Wang *et al*. [20] and analyzed the relationship between *MAP17* expression and these specific gene sets PN-GSCs are defined by Microtubule-Associated Protein 2 (*MAP2*), Delta-Like Ligand 2 (*DLL2*), Oligodendrocyte Transcription Factor 2 (*OLIG2*), SRY-Box Transcription Factor 2 (*SOX2*), Fucosyltransferase 4 (*FUT4*), and Prominin-1 (*CD133*), while MES-GSCs are defined by the expression of CD44 Antigen (*CD44*), Chitinase-3-Like Protein 1 (*CHI3L1*), Glial Fibrillary Acidic Protein (*GFAP*), Heat Shock Protein Family A (*Hsp70*) Member 5 (*HSPA5*), BMI1 Proto-Oncogene, Polycomb Ring Finger (*BMI1*), and Aldehyde Dehydrogenase 1 Family Member A3 (*ALDH1A3*) [20]. The correlation between *MAP17* and the genes was evaluated using the Spearman correlation test and visualized as a bubble plot. Similarly, we extracted the normalized expression Log2 (norm count+1) of each immune checkpoint ligand and its corresponding receptor, and assessed their distribution between the low- and high-*MAP17* groups. The selected ligand-receptor pairs are: Galectin-9 (*Gal-9*) for T-cell immunoglobulin and mucin domain-containing protein 3 (*TIM3*) and V-domain immunoglobulin suppressor of T cell activation (*VISTA*), *CD80/CD86* (*B7-1/B7-2*) for cytotoxic T-lymphocyte-associated protein 4 (*CTLA-4*), herpesvirus entry mediator (*HVEM*) for B- and T-lymphocyte attenuator (*BTLA*), programmed death-ligand 1 (*PD-L1*) for programmed cell death protein 1 (*PD-1*), CD155 for T-cell immunoreceptor with Ig and ITIM domains (*TIGIT*) and *CD96*, *4-1BB* (*CD137*) for 4-1BB ligand (*4-1BBL*), and fibrinogen-like protein 1 (*FGL1*) for lymphocyte-activation gene 3 (*LAG3*).

Gene Expression Based on GEPIA Analysis

The Gene Expression Profiling Interactive Analysis (GEPIA, http://gepia.cancer-pku.cn/) [21] is a webtool, providing gene expression, state/grade, correlation, and survival data based on the TCGA and normal Genotype-Tissue Expression (GTEx) projects. Gepia provided normalized gene expression, as transcripts per kilobase million (TPM) values. For gene comparison, the log2FC cutoff used is 1.0, and the *p*-value cutoff is 0.01. The matched normal versus GBM was performed using the "Expression DIY" module from Gepia and the log2 (TPM + 1) transformed expression data were used for plotting with a one-way analysis of variance (ANOVA) test as statistical analysis. The log2 (TPM+1) expression levels of the 24 genes from the *MKI67* downregulated set were compared between GBM and corresponding normal tissues from the GTEx database.

MAP17 Protein Expression in GBM Tissue

The Human Protein Atlas (https://www.proteinatlas.org/) is a comprehensive online resource for mapping human proteins across various compartments, including cells, tissues, and organs. It integrates data from Omics technologies, immunohistochemistry (IHC), mass spectrometry-based proteomics, and systems biology approaches. In this study, representative IHC images of MAP17 in high-grade GBM tissues were visualized, along with the percentage of protein expression. We showed three IHC staining intensities from the database with low (less than 25%), intermediate (between 25–75%), and high (higher than 75%) protein detection.

Genetic Mutation Based on TIMER 2.0 Analysis

TIMER 2.0 (http://timer.cistrome.org/) [22] is an online resource for analyzing immune infiltration and gene expression across different types of cancer. Using the module "Gene_mutation", we evaluated the *MAP17* expression levels between wild-type and mutated common genetic mutations (Isocitrate Dehydrogenase 1 (*IDH1*), Tumor Protein 53 (*TP53*), cyclin-dependent kinase inhibitor 2A (*CDKN2A*), Neurofibromin 1 (*NF1*), Epidermal Growth Factor Receptor (*EGFR*), and Phosphatase and Tensin Homolog (*PTEN*)) in GBM, and using Wilcoxon signed-rank test as statistical analysis.

Immune Cell Distribution Based on TISIDB

TISIDB [23] (http://cis.hku.hk/TISIDB/) is an online repository database for tumor and immune system interactions in 30 cancer types from the TCGA database, integrated from literature mining and high-throughput data. TISIDB provides the relative abundance of genes of interest and tumor-infiltrating immune cells for each cancer type, using gene set variation analysis (GSVA) based on gene expression profiles. It also provided the correlation between the gene of interest and immune cells, assessed using the Spearman correlation test. Therefore, we extracted the Spearman correlation coefficients between individual immune cells and each gene (e.g., *MKI67*, *CYP11A1*, *SAA1*, *CXCL5*, *SAA2*, *CHI3L2*, and *MAP17*), and visualized the results as a heatmap. Additionally, the GSVA score was

extracted for the three most represented immune cells (e.g., MDSCs, macrophages, Th1 cells) and the three less represented (e.g., activated CD4 T cells, memory B cells, and Th2 cells), and the distribution was evaluated in the low and high *MAP17* groups.

IFN-γ Gene Network via STRING

To further categorize the key interferon-gamma (*IFN-γ*) genes associated with *MAP17*, we compared two gene sets representing the IFN-γ response from Reactome and Hallmark analyses, displaying the shared and unique genes using a Venn diagram. The 22 genes common to both sets were subjected to Search Tool for the Retrieval of Interacting Genes/Proteins (STRING) (https://string-db.org/) network analysis, and Gene Ontology (GO) enrichment of DEGs was performed using the STRING database across three categories: biological processes, molecular functions, and cellular components [24]. An FDR correction was applied to account for multiple tests, with an adjusted *p*-value cutoff of <0.05. The top pathways were plotted as bar graphs with the log-transformed FDR values.

Statistical Analysis

All statistical analyses were performed using GraphPad Prism software 10.3.0.507 for Windows, (GraphPad Software, San Diego, CA USA), with data presented as the mean ± standard deviation (SD). Comparisons of gene expression between high and low MAP17 groups, including GBM subtypes, metabolic receptors, immune abundance, and immune checkpoint pairs, were conducted using a two-tailed unpaired student *t*-test. Genetic mutation distribution comparing wildtype and mutated groups was analyzed using the Wilcoxon test. Gene expression correlations, including cycling genes, stem cell markers, antigen-presenting cells, and immune cell distribution were calculated using Spearman's rank correlation coefficient, with Spearman's rho (correlation coefficient) and *p*-values presented in the figures. The Kaplan–Meier method was employed to estimate OS, DSS, and PFI for high- and low-risk patients, with differences between the survival curves evaluated using the log-rank test.

Results

MAP17 is Associated with Slow-Cycling Phenotype in GBM

To identify potential biomarkers associated with the slow-cycling phenotype in GBM, we used *MKI67* gene expression, as a proliferative marker previously published to distinguish between FCC and SCC groups. We first divided the TCGA-GBM cohort into two groups based on the median expression level of *MKI67* and performed GSEA of the TCGA-GBM dataset available on Xena. To confirm the potential of the FCC phenotype-enriched *MKI67* groups, our data showed that the top 10 upregulated pathways include several cell cycle pathways (Fig. 1A), suggesting the proliferative characteristic associated with *MKI67* high groups. Downregulated pathways were mostly related to G protein-coupled receptor (GPCR) pathways and metabolic and immune-related signatures. Based on enrichment analysis, we considered the FCC groups as *MKI67*-high, while the SCC groups were classified as *MKI67*-low. To further identify potential genes associated with slow-cycling phenotype, we selected gene expression based on DEGs with a cutoff of logFC <-1.5 and a significance threshold of $p < 0.0001$. This analysis revealed a core set of hub genes, comprising 24 genes that met these criteria. Further examination of the expression of each gene in the core set revealed that 16 genes (*CD3D*, *MAP17*, *HP*, *CYP11A1*, *CHODL*, *CHI3L1*, *CHI3L2*, *FAM183A*, *SLPI*, *LGR6*, *LTF*, *PLA2G5*, *PLA2G2A*, *PI3*, *SAA1*, *SAA2*) were significantly upregulated in GBM compared to normal, while two genes, *CCK* and *SLC39A12*, were downregulated compared to normal tissue (Fig. 1B). Next, we evaluated the prognostic significance of these 24 genes using the Xena platform to extract the OS, DSS, and PFI. Our analysis identified six genes (*MAP17*, *CHI3L2*, *SAA2*, *CXCL5*, *SAA1*, and *CYP11A1*), with *MAP17* showing the strongest prognostic value across all three survival metrics (Fig. 1C). Among these, *CHI3L2*, *SAA2*, *SAA1*, and *CXCL5* have been previously investigated as clinical biomarkers in GBM, linked to poor prognosis, therapy resistance, inflammation, and elevated immune signatures [25–28].

In this article, we extend our investigation to *MAP17*, which emerged as the most significant gene in both expression and prognostic analyses (**Supplementary Fig. 1A**). MAP17 has been shown to be preferentially expressed in slow-dividing hematopoietic cells [29]. To verify whether *MAP17* can be associated with a slow-cycling phenotype in GBM, we analyzed its correlation with two fast-cycling genes, *CDK2* and *CCNB1*, as well as with slow-cycling genes, *CDKN1A* and *G0S2*. Our results revealed a negative correlation between *MAP17* and the fast-cycling genes, while a positive correlation was observed with the slow-cycling genes (Fig. 1D). These findings suggest that *MAP17* is strongly associated with the slow-cycling phenotype in GBM.

MAP17 is Strongly Distributed in Mesenchymal Subtypes

To validate the expression of MAP17 in GBM, we analyzed its protein expression in high-grade glioma tissues using immunohistochemistry data from the Human Protein Atlas. MAP17 displayed variable protein expression, ranging from weak to strong staining, with a predominance of moderate intensity (7 cases among 12 total available) (Fig. 2A). We further investigated *MAP17* expression across different GBM subtypes: classical, proneural, and mesenchymal. Our analysis revealed that *MAP17* was significantly overexpressed in the mesenchymal subtype com-

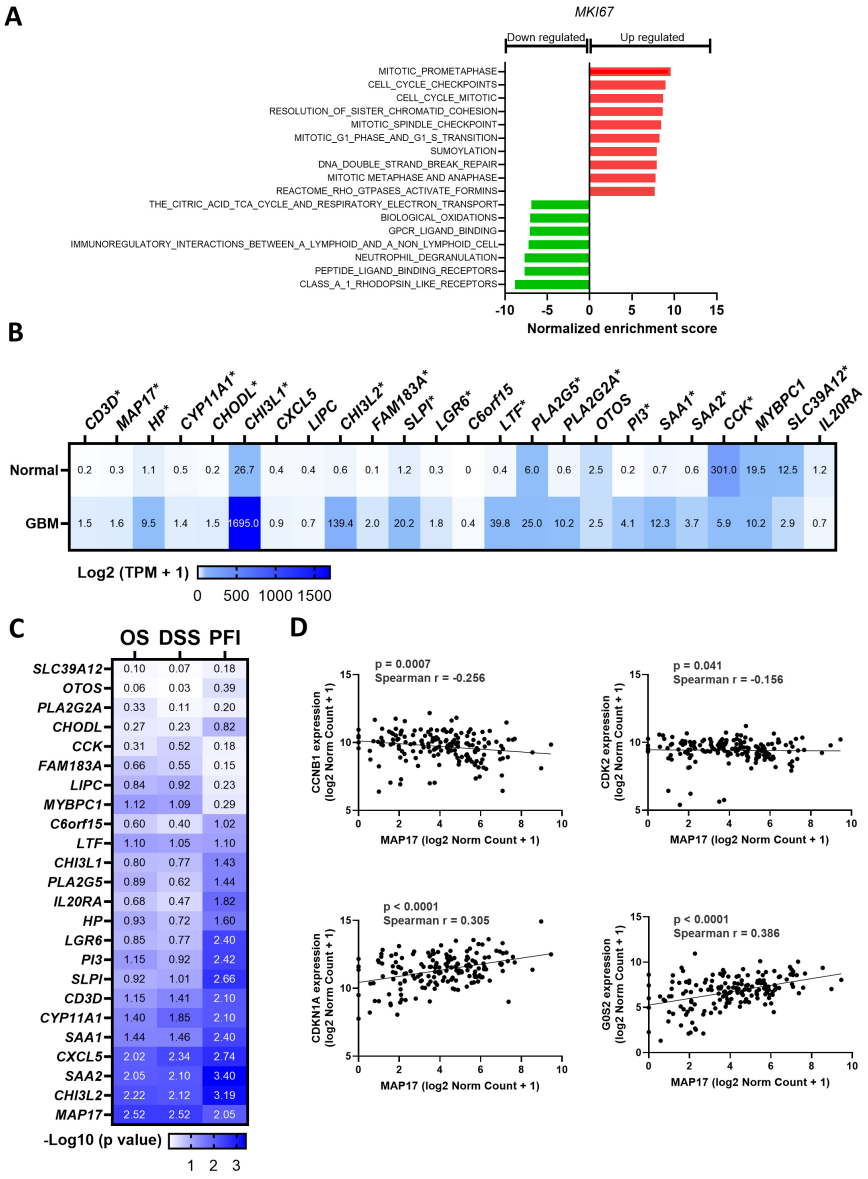

Fig. 1. Identification of Membrane-Associated Protein 17 (*MAP17*) as a potential biomarker in non-proliferative glioblastoma multiforme (GBM). (A) Gene ontology analysis of differential gene expression in high versus low *MKI67* expression GBM group based on Xena-derived GBM cohort. The most significant upregulated (red) and downregulated (green) pathways significantly enriched were plotted in normalized enrichment scores. (B) The median log2 (TPM+1) expression of 24 genes associated with slow-cycling cells (SCCs) from the *MKI67* downregulated group was compared to that of normal tissue using Gene Expression Profiling Interactive Analysis (GEPIA). Statistical analysis was conducted with a one-way analysis of variance (ANOVA), comparing normal versus GBM, and significance was set at $*p < 0.05$. (C) The -log10 *p*-value from the log-rank test was calculated for overall survival (OS), disease-specific survival (DSS), and progression-free interval (PFI) in the 24 core genes within the Xena-derived GBM cohort. (D) Spearman correlation *MAP17* expression with fast-cycling genes (*CCNB1* and *CDK2*) and slow-cycling genes (*CDKN1A* and *G0S2*) genes by plotting Log2 (norm count+1) for each marker. *CCNB1*, cyclin B1; *CDK2*, cyclin-dependent kinase 2; *CDKN1A*, cyclin-dependent kinase inhibitor 1A; *G0S2*, G0/G1 switch gene 2; *C6orf15*, Chromosome 6 Open Reading Frame 15; *CCK*, Cholecystokinin; *CD3D*, CD3 Delta Subunit; *CHI3L1*, Chitinase-3-Like Protein 1; *CHI3L2*, Chitinase-3-Like Protein 2; *CHODL*, Chondrolectin; *CYP11A1*, Cytochrome P450 Family 11 Subfamily A Member 1; *CXCL5*, C-X-C Motif Chemokine Ligand 5; *FAM183A*, Family With Sequence Similarity 183 Member A; *HP*, Haptoglobin; *IL20RA*, Interleukin 20 Receptor Subunit Alpha; *LGR6*, Leucine-Rich Repeat-Containing G Protein-Coupled Receptor 6; *LIPC*, Lipase C, Hepatic Type; *LTF*, Lactotransferrin; *MAP17*, Membrane-Associated Protein 17; *MYBPC1*, Myosin Binding Protein C1; *OTOS*, Otospiralin; *PI3*, Peptidase Inhibitor 3; *PLA2G5*, Phospholipase A2 Group V; *PLA2G2A*, Phospholipase A2 Group IIA; *SAA1*, Serum Amyloid A1; *SAA2*, Serum Amyloid A2; *SLPI*, Secretory Leukocyte Peptidase Inhibitor; *SLC39A12*, Solute Carrier Family 39 Member 12; *MKI67*, marker of proliferation KI67.

pared to the others (Fig. 2B). To investigate the pathways associated with *MAP17*, we performed GSEA by comparing the low-*MAP17* and high-*MAP17* groups, categorized based on median gene expression levels (**Supplementary Fig. 1B**). We found that the *MAP17*-high group was strongly associated with a mesenchymal signature, compared to other subtype-enriched pathways (Fig. 2C), suggesting that high *MAP17* expression is associated with a mesenchymal profile. Additionally, we examined the relationship between *MAP17* expression and key genetic mutations in GBM, including *IDH1*, *TP53*, *CDKN2A*, *NF1*, *EGFR*, and *PTEN*. Our results indicated that *MAP17* expression mostly occurred in the wild-type genetic alteration and there was no significant association with any mutated group (Fig. 2D).

MAP17 is Significantly Correlated with Mesenchymal Stem-Like Phenotype

Given the association of *MAP17* with cellular quiescence, we next investigated whether the *MAP17*-high group exhibited stemness properties. Our enrichment analysis revealed significant enrichment in canonical biological processes linked to stem cell activity, including hematopoietic stem cell differentiation ($p = 0.0013$), pluripotent stem cell differentiation pathways ($p = 0.009$), and general stem cell pathways ($p = 0.03$) (Fig. 3A). Additionally, we focused on the enrichment of stem cell marker pathways by comparing *MAP17*-high and *MAP17*-low groups. Our analysis demonstrated strong enrichment of several stem cell signaling pathways in GBM, including the nuclear factor erythroid 2-related factor 2 (*NRF2*) pathway ($p < 0.0001$), integrin 3 pathway ($p = 0.001$), CXC chemokine receptor 4 (*CXCR4*) pathway ($p = 0.003$), and urokinase plasminogen activator surface (*uPA*)-urokinase plasminogen activator surface receptor (*uPAR*) pathway ($p = 0.007$) (Fig. 3A) [30–33]. Correlation analysis between *MAP17* and these stem cell markers indicated a significant overall association (Fig. 3B). We further explore the association of *MAP17* with the two GSCs subtypes, PN-GSCs and MES-GSCs. PN-GSCs are phenotypically characterized by the expression of *MAP2*, *DLL2*, *OLIG2*, SOX2, *FUT4*, and *CD133*, while MES-GSCs are defined by the expression of *CD44*, *CHI3L1*, *GFAP*, *HSPA5*, *BMI1*, and *ALDH1A3*. Our Spearman correlation analysis revealed that *MAP17* is strongly correlated with five markers associated with MES-GSCs including *CD44*, *CHI3L1*, *GFAP*, *HSPA5*, and *ALDH1A3* (Fig. 3C) but not with the PN-GSC markers.

To explore the association of *MAP17* with SCCs, we examined the main metabolic pathways enriched in the *MAP17*-high group. Our analysis revealed significant enrichment in pathways related to folate, zinc, fatty acids, vitamins, and glycogenesis (Fig. 3D, Table 1 and **Supplementary Table 1**).

Notably, aerobic glycolysis ($p = 0.12$) and oxidative phosphorylation ($p = 0.38$), which are typically enriched in fast-cycling cells, did not show significant enrichment. To validate these findings, we assessed the expression of key transporters involved in these metabolic processes in the *MAP17*-high and *MAP17*-low groups. We selected several transporters known to play crucial roles in GBM and the nervous system, including Folate Receptor 1 (*FOLR1*) and Folate Receptor 2 (*FOLR2*) for folate metabolism, *SLC39A4* and *SLC39A12* for zinc metabolism, and *ACSL4* and *ACSL5* for fatty acid metabolism [34–37]. These transporters were also identified within the hub gene sets of metabolic-related pathways (Table 1). All these transporters were significantly upregulated in the *MAP17*-high group compared to the low *MAP17* group (Fig. 3E). These results indicate that *MAP17* is strongly associated with a quiescent stemness phenotype characterized by specific metabolic processes.

MAP17 is Correlated with IFN-γ-Related Immune Signature

We conducted Reactome and Hallmark enrichment analyses to identify the pathway enrichment associated with the high versus low *MAP17* groups. The most significant Hallmark pathway identified was the *IFN-γ* response (Fig. 4A), which was also highly represented in the Reactome analysis as the third most significant pathway (Fig. 4B). In the Reactome enrichment analysis, peptide ligand-binding receptors were highly enriched in the high *MAP17* group, consistent with findings in the downregulated *MKI67* group (Fig. 1A). Moreover, we observed an enrichment of several cytokine signaling related to inflammation such as Tumor Necrosis Factor Alpha (*TNF-α*), Interferon Alpha (*IFN-α*), Interleukin 6 (*IL-6*), Interleukin 2 (*IL-2*), and Interleukin 1 (*IL-1*) (Fig. 4A). Additional pathways include immune processes such as complement signaling, and antigen presentation processing. Interestingly, the *MAP17* high group exhibited several resistance mechanisms such as epithelial-mesenchymal transition (EMT), chemokine receptors-chemokine signaling, and hypoxia. Overall, *MAP17* seems to be associated with several pathways involved in inflammation and immune processes.

To further investigate key genes involved in IFN-γ signaling, we performed an intersection analysis between the IFN-γ signaling pathways from both the Hallmark and Reactome gene sets. This analysis identified 22 overlapping genes, as depicted in the Venn diagram (Fig. 4B). These 22 genes, central to the IFN-γ signaling module, were then analyzed for protein-protein interactions using the STRING database (Fig. 4C). To gain deeper insights into the roles of these 22 candidate genes within IFN-γ-related networks, we performed GO functional and pathway enrichment analysis using the STRING database. The enrichment analysis revealed a strong association with immune system processes, particularly those related to MHC class I and II, which are critical for antigen presentation signaling (Fig. 4D). These findings suggest that *MAP17* is

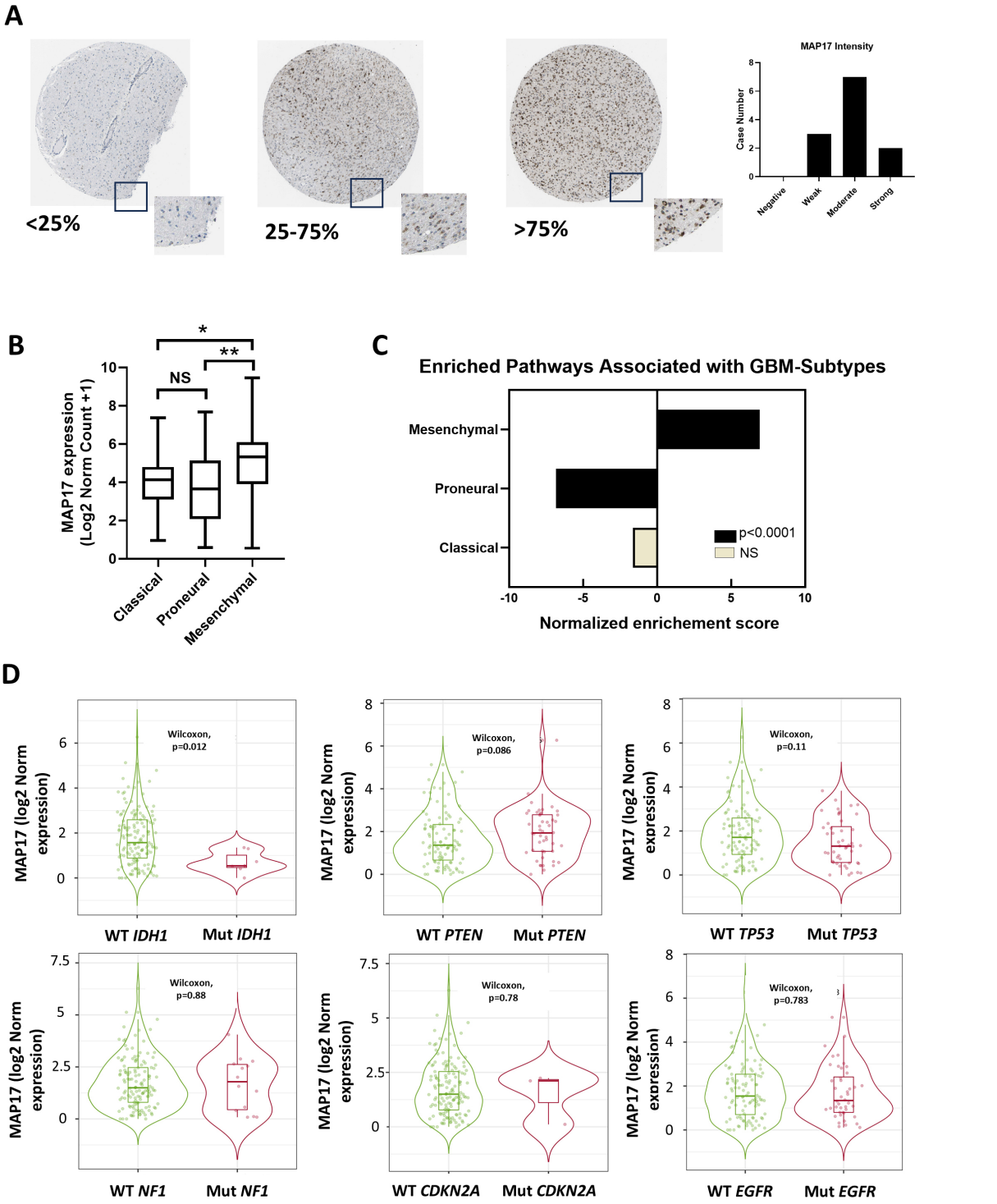

Fig. 2. Histopathology and clinical relevance of MAP17 in GBM. (A) Representative of immunohistochemistry image of different protein MAP17 level expression retrieved from the Human Proteome Atlas. The high-magnified region is displayed with the corresponding percentage of detection. Bar charts summarized the number of cases with different immunohistochemistry (IHC) staining intensities. (B) The log2-transformed normalized gene expression of *MAP17* in different TCGA-GBM subtypes: classical, proneural, and mesenchymal. The statistical test was performed using unpaired *t*-tests. *$p < 0.05$, **$p < 0.01$, NS, non-significant. (C) Enrichment analysis of GBM subtype-associated pathways in the high-*MAP17* group was conducted using Xena-GSEA. The nominal *p* value was indicated with a code color. NS, non-significant. (D) *MAP17* gene distribution between wild type (WT, green) and the main genetic mutations (Mut, red) in GBM. A statistical test was performed to compare WT versus mutated genes using the Wilcoxon test, and the *p*-value is shown on the graph. GSEA, gene set enrichment analysis; *IDH1*, Isocitrate Dehydrogenase 1; *TP53*, Tumor Protein 53; *CDKN2A*, cyclin-dependent kinase inhibitor 2A; *NF1*, Neurofibromin 1; *EGFR*, Epidermal Growth Factor Receptor; *PTEN*, Phosphatase and Tensin Homolog.

Table 1. Summary of metabolic-related pathways enriched in Membrane-Associated Protein 17 (*MAP17*).

Term	NES	*p*-value	FDR	Gene ID
Folate metabolism	3.6184	0.0003	0.0093	*SAA2*, *SAA1*, *CSF1*, *SERPINA3*, *SERPINE1*, *FOLR2*, *FOLR1*, *MTHFS*, *HBB*, *SOD2*, *SOD3*, *IL6*, *HBA1*, *CCL2*, *ICAM1*, *IL1B*
Zinc homeostasis	3.3921	0.0007	0.0183	*SLC39A12*, *MT1F*, *MT1E*, *MT3*, *MT1L*, *MT1X*, *MT1G*, *MT1H*, *SLC39A8*, *MT1M*, *SLC39A4*, *MT1A*, *MT2A*
Fatty acid metabolism	3.3367	0.0008	0.020	*ALOX15B*, *THEM4*, *ACADS*, *AMACR*, *ALOX5*, *GGT1*, *CBR1*, *ACADVL*, *MMAA*, *ACOX2*, *AKR1C3*, *PTGDS*, *DPEP2*, *ACOT13*, *CROT*, *ACADL*, *MID1IP1*, *CYP4F11*, *GGT5*, *GPX4*, *ALOX5AP*, *PTGES*, *PON3*, *CYP4F3*, *PON2*, *ELOVL7*, *GPX1*, *ACSF2*, *ACSL4*, *ACAA2*, *LTC4S*, *CYP2J2*, *HPGDS*, *ACSL5*, *ACSL6*, *MAPKAPK2*, *CYP1B1*, *TBXAS1*, *SLC22A5*, *ACOT11*, *PTGS2*, *ACBD4*, *PPT1*, *PTGR1*, *ABCC1*, *NUDT7*, *ACADM*, *ACOT4*, *ACSL1*, *PTGR2*, *HSD17B8*, *SLC25A20*, *PHYH*, *PTGS1*, *PECR*, *CYP2U1*, *ELOVL1*, *HSD17B12*, *HSD17B3*, *EPHX2*, *ECHS1*, *ACOT9*, *ABCD1*, *PRKAG2*, *ACACB*, *ALDH3A2*
Metabolism of vitamins and cofactors	3.041	0.0024	0.036	*BCO2*, *RETSAT*, *PPCS*, *APOE*, *VNN1*, *RBP4*, *NAMPT*, *APOC2*, *AKR1C3*, *ACP5*, *GPC4*, *LMBRD1*, *AKR1C1*, *SPR*, *RBP1*, *MOCOS*, *NNMT*, *PLB1*, *GCH1*, *LRP2*, *GCHFR*, *GPC5*, *TPK1*, *PARP8*, *SLC19A3*, *GSTO1*, *QPRT*, *PARP9*, *SLC25A19*, *ALDH1L1*, *SDC2*, *RNLS*, *VNN2*, *GSTO2*, *LRAT*, *NMNAT3*, *PTGS2*, *PARP14*, *PARP10*, *CD38*, *FOLR2*, *MTHFS*, *PNPO*, *BST1*, *SDC4*, *SLC2A3*, *PRSS3*, *AOX1*
Glycolysis gluconeogenesis	2.376	0.0175	0.111	*HK3*, *PCK2*, *PGAM2*, *ALDH9A1*, *ALDH7A1*, *ALDH2*, *GCK*, *ALDH3B1*, *GALM*, *ALDH3A1*, *ALDOA*, *HK2*, *ENO2*, *LDHA*, *FBP1*, *PGK1*

NES, Normalized Enrichment Score; FDR, false discovery rate; Gene ID, Gene Identification. The full names of the gene abbreviations are provided in **Supplementary Table 1**.

linked to inflammatory responses, such as IFN-γ signaling, with significant enrichment in immune response processes.

MAP17 is Associated with a Strong Immunosuppressive Environment

To assess the relationship between antigen presentation and *MAP17*, we analyzed the correlation between *MAP17* expression and APCs such as dendritic cells, macrophages, and B cells using the TISIDB web portal. Our analysis revealed a strong correlation with all three types of APCs, particularly macrophages (Fig. 5A).

We further expanded our investigation to explore additional immune-related pathways associated with *MAP17*. We observed significant enrichment of several inflammatory immune cells, including T helper cells, cytotoxic lymphocytes (CTLs), natural killer T (NKT) cells, monocytes, dendritic cells, granulocytes, and neutrophils (Fig. 5B). To gain deeper insights into immune cell infiltration associated with *MAP17*, we conducted a comparative analysis between *MKI67*, and six genes enriched in the *MKI67*-downregulated hub, relative to *MAP17*. This comprehensive comparison revealed distinct differences in immune cell distribution between the high *MKI67* group and the other genes. Among the immune cells highly enriched in the *MAP17* group, we identified MDSCs, macrophages, and Th1 cells (Fig. 5C). Notably, MDSCs, macrophages, and Th1 cells were significantly more abundant in the high *MAP17* group compared to the low *MAP17* group (Fig. 5D). The significance of Th1 cells in the context of high *MAP17* expression may be linked to their role as a key source of IFN-γ production [38]. Conversely, immune cells such as activated CD4+ T cells, memory B cells, and Th2 cells were less prevalent in the high *MAP17* group (Fig. 5D). To further evaluate the immunosuppressive environment associated with *MAP17*, we analyzed the expression of various immune checkpoint ligands and their respective receptors in the low versus high *MAP17* groups. Our analysis revealed a significant increase in several inhibitory receptors, including *TIM3*, *TIGIT*, *CD96*, *CTLA-4*, *BTLA*, *PD-1*, and *VISTA*, with *TIM3* being highly represented (Fig. 5E). Correspondingly, their ligands were also upregulated, such as *Gal-9* for *TIM3* and *VISTA, CD80/CD86* for *CTLA-4, HVEM* for *BTLA,* and *PD-L1* for *PD-1* (Fig. 5F). However, *CD155*, the ligand for *TIGIT* and *CD96*, did not show any significant difference in expression. Additionally, the activating immune checkpoint pair *4-1BBL*/*4-1BB* was also elevated in the high *MAP17* group, while no differences were observed for the FGL1/LAG3 pair (Fig. 5E,F).

Overall, these findings suggest that *MAP17* is associated with an immunosuppressive environment characterized by the enrichment of immune checkpoint inhibitory pairs.

Discussion

While considerable progress has been made in understanding GBM, the heterogeneity of GBM necessitates continued research to identify novel biomarkers for more personalized and targeted therapies. Bioinformatic approaches significantly accelerate precision oncology by analyzing tumor heterogeneity and detecting relevant patterns to identify potential targets. These computational methods pave the way for biomarker prediction before experimental validation, saving time, resources, and biological materials, while accelerating the overall research and discovery process. In this study, we used a bioinformatic approach to identify *MAP17* as a novel biomarker linked to

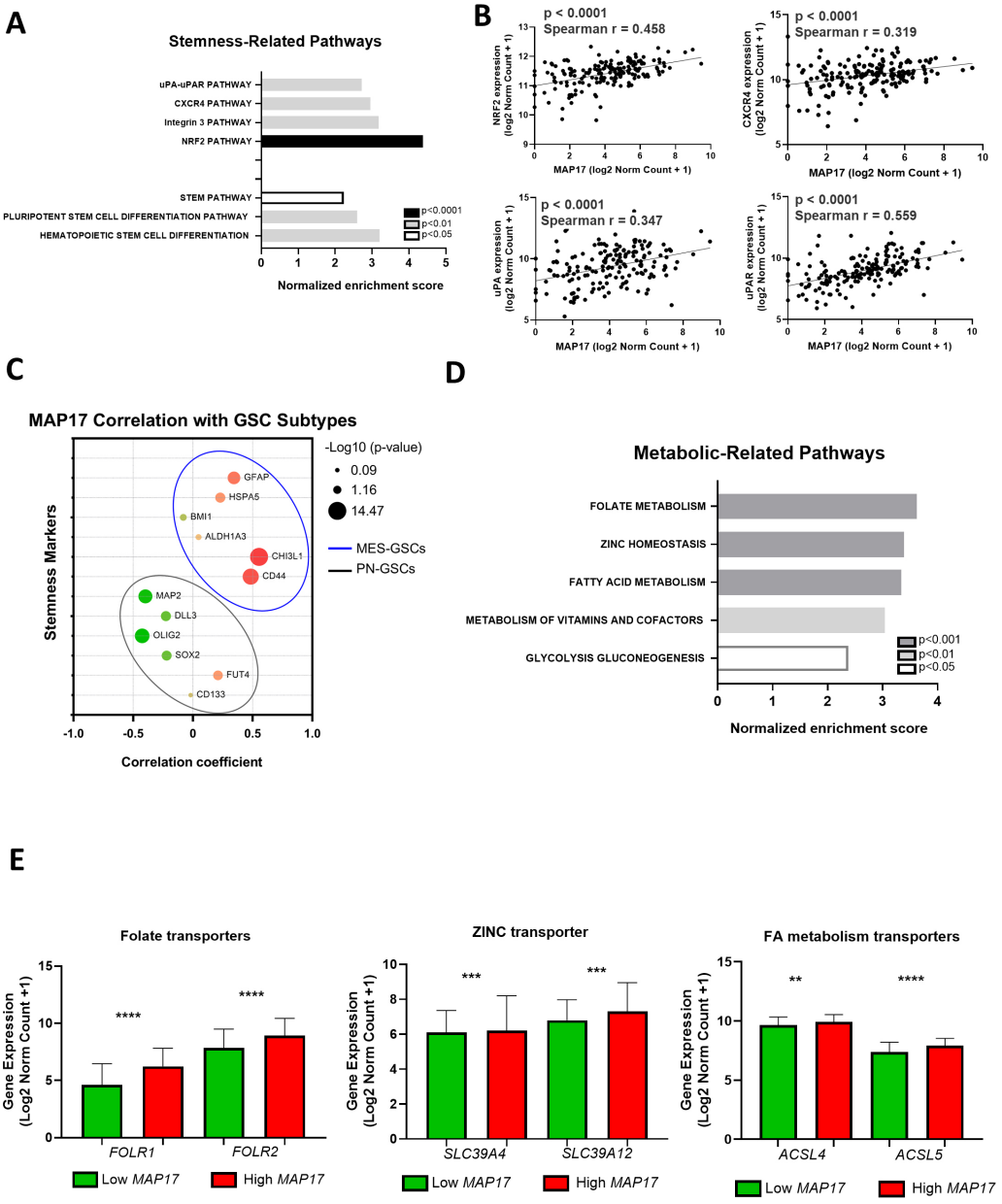

Fig. 3. High MAP17 expression associated with cancer stem cells and metabolic processes. (A) Enrichment analysis associated with stemness pathways enriched in the *MAP17* group with the nominal *p*-value shown with code color. (B) Spearman correlation between *MAP17* expression with GBM stem cell markers by plotting Log2 (norm count+1) for each marker. (C) The bubble plot illustrates the Spearman correlation between each marker and *MAP17*. It displays the normalized Log2 (norm count+1) expression of proneural GBM stem cell (PN-GSC) and mesenchymal GBM stem cell (MES-GSC) markers in relation to the normalized Log2 (norm count+1) expression of *MAP17*. The size of the bubbles represents the correlation coefficient, and statistical significance is indicated by the -log10 *p*-value. (D) Metabolic-related pathways were assessed by Xena-derived GSEA analysis with a nominal *p*-value shown with code color. (E) Distribution of metabolic transporters involved in folate, zinc, and fatty acid pathways comparing low versus high *MAP17* groups. Statistical analysis was performed comparing low and high groups for each transporter using an unpaired *t*-test, ****$p < 0.0001$, ***$p < 0.001$, **$p < 0.01$. *SLC39A4*, Solute Carrier Family 39 Member 4; *SLC39A12*, Solute Carrier Family 39 Member 12; *ASCL5*, Acyl CoA synthetase 5; *ASCL4*, Acyl CoA synthetase 4; *NRF2*, nuclear factor erythroid 2-related factor 2; *CXCR4*, CXC chemokine receptor 4; *uPA*, urokinase plasminogen activator surface; *uPAR*, urokinase plasminogen activator surface receptor; *GFAP*, Glial Fibrillary Acidic Protein; *HSPA5*, Heat Shock Protein Family A (*Hsp70*) Member 5; *BMI1*, BMI1 Proto-Oncogene, Polycomb Ring Finger; *ALDH1A3*, Aldehyde Dehydrogenase 1 Family Member A3; *CHI3L1*, Chitinase-3-Like Protein 1; *MAP2*, Microtubule-Associated Protein 2; *DLL3*, Delta-like ligand 3; *OLIG2*, Oligodendrocyte Transcription Factor 2; *SOX2*, SRY-Box Transcription Factor 2; *FUT4*, Fucosyltransferase 4.

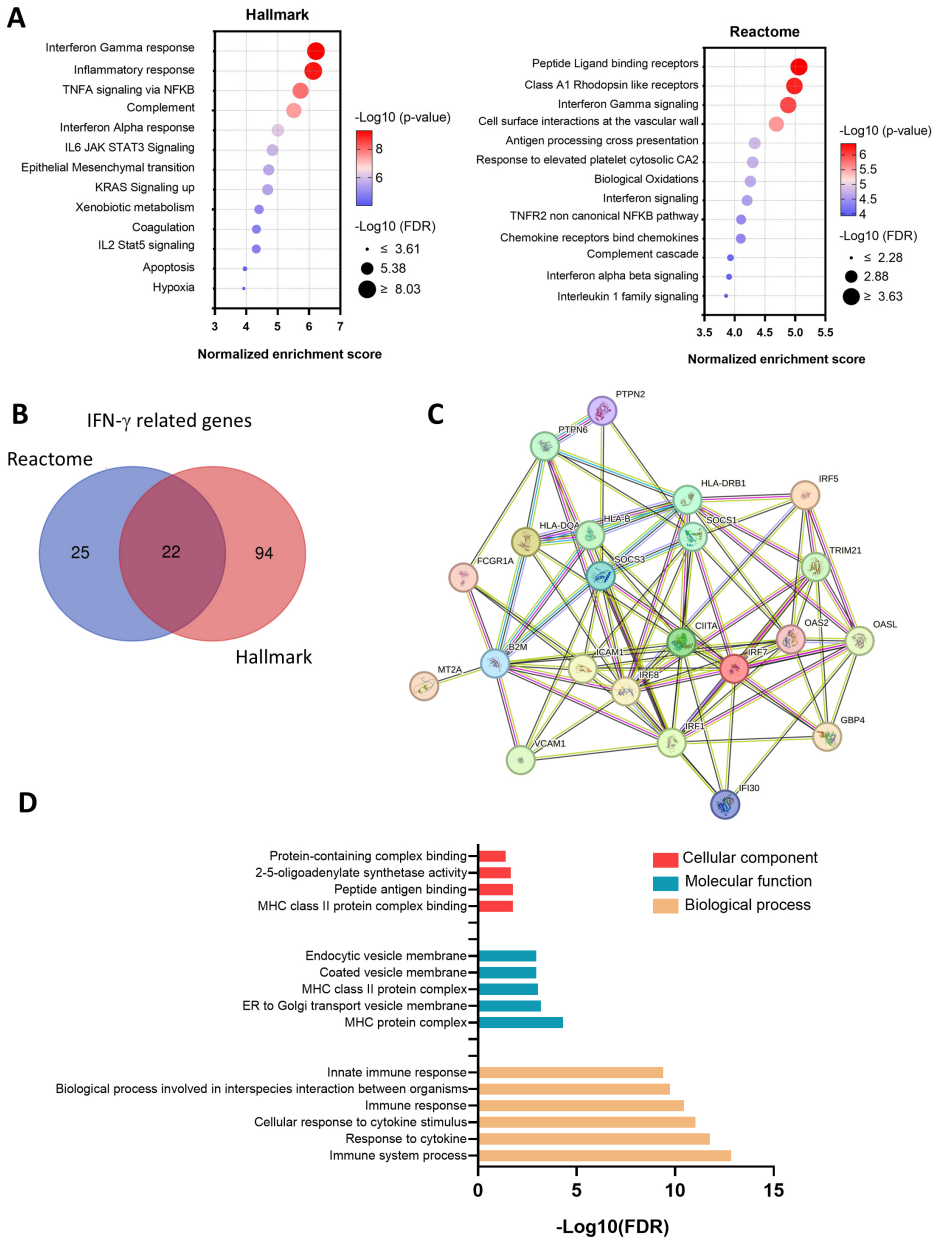

Fig. 4. MAP17 associated with IFN-γ-related genes and strong immune response. (A) The top significant Hallmark and Reactome gene sets were upregulated in the *MAP17* group from Xena-GSEA analysis. The size of the dot indicates significance (proportional to the GSEA -log10 FDR value). Blue and red indicate the significance of -log10 (*p*-value) for enrichment pathways. (B) The C-Venn diagram represents the shared and unique gene number among the IFN-γ response in Reactome and Hallmark signature. (C) Network analysis using Search Tool for the Retrieval of Interacting Genes/Proteins (STRING) representing the interaction between the 22 hub genes shared between Reactome and Hallmark of IFN-γ pathways. (D) Gene Ontology (GO) enrichment of biological, molecular, and cellular components was assessed for the 22 IFN-γ hub gene sets via the STRING database. The bar graph represents -log10-transformed false discovery rate (FDR) values, retrieved from STRING analysis. *VCAM1*, Vascular Cell Adhesion Molecule 1; *IRF5*, Interferon Regulatory Factor 5; *OAS2*, 2′-5′-Oligoadenylate Synthetase 2; *IFI30*, Interferon Gamma Inducible Protein 30; *HLA-DRB1*, Major Histocompatibility Complex Class II DR Beta 1; *ICAM1*, Intercellular Adhesion Molecule 1; *IRF1*, Interferon Regulatory Factor 1; *SOCS3*, Suppressor of Cytokine Signaling 3; *HLA-B*, Major Histocompatibility Complex Class I B; *MT2A*, Metallothionein 2A; *IRF7*, Interferon Regulatory Factor 7; *OASL*, 2′-5′-Oligoadenylate Synthetase Like; *CIITA*, Class II Major Histocompatibility Complex Transactivator; *GBP4*, Guanylate Binding Protein 4; *FCGR1A*, Fc Fragment of IgG Receptor Ia; *SOCS1*, Suppressor of Cytokine Signaling 1; *HLA-DQA1*, Major Histocompatibility Complex Class II DQ Alpha 1; *TRIM21*, Tripartite Motif Containing 21; *B2M*, Beta-2-Microglobulin; *PTPN6*, Protein Tyrosine Phosphatase Non-Receptor Type 6; *PTPN2*, Protein Tyrosine Phosphatase Non-Receptor Type 2; *IRF8*, Interferon Regulatory Factor 8.

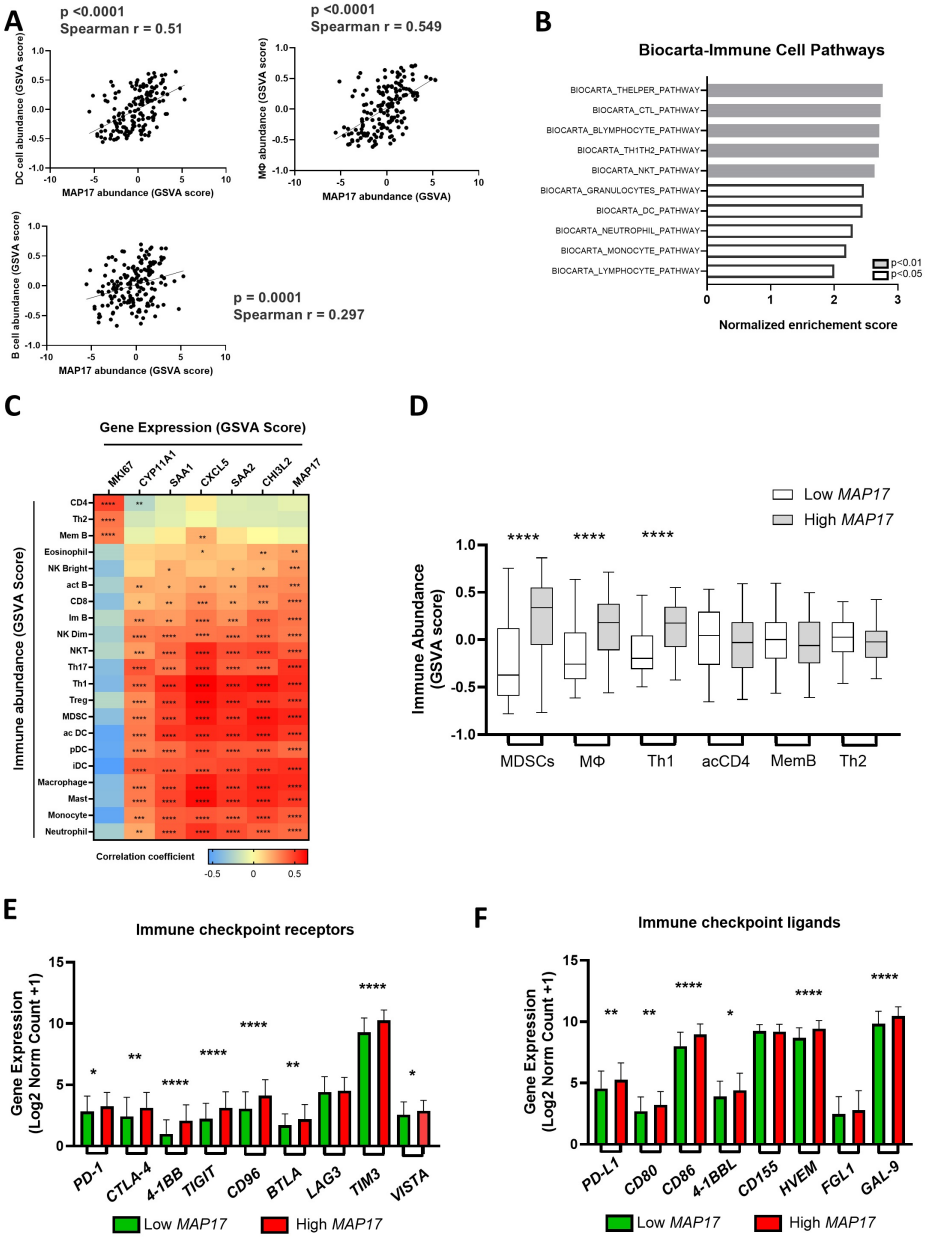

Fig. 5. The association between *MAP17* and the immune microenvironment in GBM. (A) Spearman correlation of GSVA scores was used to compare *MAP17* expression with the presence of antigen-presenting cells, including macrophages, dendritic cells, and B cells. (B) GSEA enrichment of Biocarta focussing on immune cell pathways enriched in a high *MAP17* group with the nominal *p-value* shown in code color. (C) Spearman correlation heatmap between GSVA score of immune cells and single-cell marker genes including *MKI67*, *CYP11A1*, *SAA1*, *CXCL5*, *SAA2*, *CHI3L2*, and *MAP17*. Statistical test was performed with Spearman correlation test, $****p < 0.0001$, $***p < 0.001$, $**p < 0.01$, $*p < 0.05$. (D) The distribution of immune cells, based on GSVA scores, was compared between the low (white) and high (gray) *MAP17* groups. The graph focused on the three most represented immune cells (MDSCs, macrophages, and Th1) and the three least represented cells (activated CD4, memory B, and Th2). Statistical analysis was performed using unpaired *t*-tests, with significance indicated as $****p < 0.0001$. (E) The distribution of immune checkpoint receptors was assessed by plotting the log2 (normalized count + 1) ligand expression in the low versus high *MAP17* groups. (F) The distribution of immune checkpoint ligands was compared based on log2 (normalized count + 1) expression in the low (green) and high (red) *MAP17* groups. Statistical analysis was conducted comparing each molecule between low and high groups using unpaired *t*-tests, with significance indicated as $****p < 0.0001$, $**p < 0.01$, $*p < 0.05$. MDSCs, myeloid-derived suppressor cells; *PD-1, programmed cell death protein 1*; *CTLA-4, cytotoxic T-lymphocyte associated protein 4*; *4-1BB*, *CD137*; *TIGIT*, T-cell immunoreceptor with Ig and ITIM domains; *BTLA*, B- and T-lymphocyte attenuator; *LAG3*, lymphocyte-activation gene 3; *TIM3*, T-cell immunoglobulin and mucin domain-containing protein 3; *VISTA*, V-domain immunoglobulin suppressor of T cell activation.

slow-cycling cells in GBM. *MAP17* correlates with markers of slow-cycling like phenotype, stemness, and is enriched in a mesenchymal stem-cell-like subtype with active metabolic pathways. Our investigation revealed that *MAP17* is strongly associated with poor outcomes, high-grade gliomas, and aggressive features. It also shows significant enrichment in IFN-γ-related pathways and an immunosuppressive microenvironment, highlighting its potential as a therapeutic target in GBM.

MAP17, also known as DD96 or PDZK1IP1, is a small membrane-bound protein primarily localized at the plasma membrane and the Golgi apparatus. It functions as a cargo protein, facilitating the transport of various molecules from the Golgi to the cell membrane. MAP17 interacts with PDZ domain-containing proteins, such as PDZK1, influencing the activity of these proteins and aiding in their transport across the plasma membrane [39]. This protein is found at cell-cell junctions and plays a role in several critical biological processes, including signal transduction, cellular transport, and the maintenance of cell polarity [40]. MAP17 is notably upregulated in various cancers, including those of epithelial origin (carcinomas), mesenchymal origin (sarcomas), and in neoplasia such as lymphomas and glioblastomas [41]. Its overexpression is frequently associated with more aggressive tumor phenotypes and poor clinical outcomes. MAP17 has been linked to the activation of pro-tumorigenic signaling pathways, which promote cell survival, proliferation, and metastasis despite lacking any enzymatic or transcriptional activity [41,42].

Several studies demonstrated the role of MAP17 in increasing tumorigenesis in various cancers. MAP17, through its cargo role, has been shown to propagate EMT, stemness, and metastasis in breast cancer by being transported to recipient cells via exosomes [43]. Another mechanism by which MAP17 induces EMT, as observed in papillary thyroid carcinoma, involves the upregulation of extracellular matrix molecules and signaling pathways that promote proliferation and metastasis [44]. An additional hallmark of tumor aggressiveness is its inherently hypoxic nature. Dong *et al*. [45] demonstrated a reciprocal interaction between hypoxia and MAP17. Mechanistically, hypoxia upregulates MAP17 expression in hepatocellular carcinoma (HCC), while elevated MAP17 levels enhance tumor aggressiveness by modulating intracellular reactive oxygen species (ROS), which in turn activate the downstream effectors of hypoxia, HIF1α [45]. MAP17 also participates in stemness properties. For example, overexpression of MAP17 in breast cells or conditioned media increases the number and size of CD44+ cancer stem cells (CSCs), partly through exosome-mediated transport to neighboring cells [43] or by enhancing Notch and stem cell-related pathways both *in vitro* and *in vivo*. This mechanism may be shared across several human cancers, such as lung, breast, and colon, where a positive correlation between MAP17 and signatures of Notch and stem cell pathways has been observed [46]. Moreover, MAP17 contributes to resistance against tumor kinase inhibitors by promoting CSC activity in lung cancer [47].

One crucial mechanism for stem cell maintenance is the requirement of a functional metabolism. For instance, aberrant folate metabolism is associated with the differentiation of GBM cells into a stem cell-like state [48,49]. Targeting folate metabolism with chemotherapy drugs demonstrated specific cytotoxicity of GSCs without affecting normal cells, both *in vitro* and *in vivo* [50]. The role of zinc pathways in stemness appears to be context dependent. In lung cancer, zinc suppresses stemness programming [51], whereas it enhances the self-renewal properties of mesenchymal stem cells derived from the human umbilical cord [52]. Metabolism is a key pathway distinguishing GSC subclones. FSCs primarily rely on glycolysis, while SCCs depend on oxidative phosphorylation and lipid metabolism for energy and survival. Notably, inhibiting fatty acid transporters in SCCs reduces invasion and tumor growth *in vivo*, suggesting that targeting metabolic mediators can be a promising approach to treat specifically SCCs. Similar metabolic discrepancies exist between PN-GSCs and MES-GSCs, with glycolytic pathways enriched in MES-GSCs but not PN-GSCs [53]. GSCs also exploit metabolic plasticity, such as the Warburg effect, switching from oxidative phosphorylation to aerobic glycolysis, driven by hypoxia-induced HIF-1α activation. MAP17 enhances the Warburg effect in HCC by stabilizing HIF-1α under hypoxia and disrupting pathways related to the cell cycle, ROS metabolism, and differentiation when inhibited [45]. Additionally, MAP17's preferential expression in slow-dividing hematopoietic cells suggests its potential role in regulating slow-cycling clones in GBM, warranting further investigation [29]. The multiple metabolic programming associated with GSCs suggested plastic metabolic reprogramming, adding another layer of complexity to these clones. Further validation is needed to evaluate the efficacy of MAP17 inhibition in targeting resistant GBM subclones. Techniques such as RNA interference (siRNA) or CRISPR/Cas9 can be used to achieve temporary or permanent *MAP17* knockdown in GBM cells. Sphere formation assays can then assess the self-renewal capacity of CSCs by monitoring sphere number, size, metabolic activity, and proliferation rates. Flow cytometry can evaluate cell cycle distribution, while *in vivo* studies using immunocompromised mice can examine tumor initiation and growth kinetics. These experiments will provide critical insights into MAP17's role in tumor growth, self-renewal, and GBM progression.

MAP17 has emerged as a predictive biomarker for therapy response. Rivero *et al*. [54] demonstrated that high MAP17 expression, combined with the phosphorylated form of DNA damage marker, pH2AX, correlates with poor prognosis after preoperative chemoradiotherapy due to enhanced DNA damage repair pathways. *In vitro*,

the DNA damage inhibitor Olaparib re-sensitized MAP17-pH2AX rectal cancer cells to radiotherapy. Similarly, *in vivo* sarcoma models treated with Olaparib and doxorubicin showed improved survival in tumors with high MAP17 and pH2AX levels [55]. Furthermore, high MAP17 expression increased sensitivity to cisplatin and bortezomib in breast and lung cancer cells *in vitro* [56,57]. Additional investigation will be required to assess the clinical significance of MAP17 and its potential as a biomarker for guiding therapeutic responses in GBM. Studies involving large cohorts of both untreated and treated patients will be essential to validate its utility in precision medicine.

MAP17 is also implicated in enhancing inflammation and immune tumor chemotaxis by facilitating the excessive transport of molecules into the tumor microenvironment. A bioinformatic analysis by Garcia-Heredia *et al.* [58] demonstrated that MAP17 overexpression in cervical, breast, and lung cancers was associated with the upregulation of several inflammation-related genes, including MHC genes, cytokines like IL-1 and IL-6, and cytokine receptors such as IFN-γ receptors. Additionally, elevated MAP17 expression increases IL-6 levels and enhances the expression of various HLA classes *in vitro* [58]. Notably, pro-inflammatory cytokines like IL-1 and IL-6 have been shown to promote glioma tumorigenesis and immune evasion by recruiting MDSCs [59]. Moreover, GSCs evade immune destruction by disrupting MHC antigen processing, leading to reduced recognition by cytotoxic CD8 T cells [60]. Interestingly, MAP17 expression has been shown to be upregulated by stimuli from T helper cytokines, including IFN-γ, IL-4, IL-6, IL-17, and IL-22 [61]. Our analysis revealed similar trends, showing a strong association between MAP17 and inflammation through MHC class I and II antigen presentation and cytokine signaling pathways. This suggests that SCCs selectively increase MAP17 in response to immune response and proinflammatory cytokines to increase immunosuppression and evade immune surveillance. To validate similar findings in GBM, MAP17 can be selectively inhibited or overexpressed in GBM cells, before the assessment of several immune evasion mechanisms such as MHC class I/II expression, infiltration of immunosuppressive cells, and pro-tumoral cytokine responses. These can be measured using qRT-PCR for gene expression, Western blot for protein levels, and ELISA or Luminex for cytokine quantification.

The increase in immune checkpoint receptors and their ligands in GBM is a mechanism by which GBM enhances the tumor's capacity to evade immune surveillance but also impairs the effectiveness of immune responses and immunotherapy [62]. For instance, GBM increases TIM3 expression to promote invasion and migration by preserving self-renewal properties *in vivo*. This upregulation also drives a pro-tumorigenic shift by recruiting TAMs through the TIM3/IL-6 signaling axis. Inhibition of TIM3/IL-6 interactions with IL-6 receptor blockers significantly reduced tumor growth *in vivo* [63]. A Phase I clinical trial combining anti-PD1 and anti-TIM3 therapies demonstrated tolerable toxicity and some anti-tumoral activity (NCT03961971) [64]. Immune checkpoint therapies targeting PD-1/PD-L1 and CTLA-4 have shown promise in various cancers but remain limited in GBM due to its immunosuppressive microenvironment. This highlights the need for identifying additional immune checkpoints to enhance the efficacy of ICIs. CD96, linked to poorer survival in glioma and GBM patients, is associated with *IDH* wild-type and mesenchymal subtypes and correlates with other checkpoints like PD-1, CTLA-4, TIM3, and TIGIT, suggesting potential synergistic effects [65,66]. Predominantly expressed on T cells, NK cells, and NKT cells, CD96 inhibition has shown promise in preclinical models, where it enhances anti-PD-1 therapy by boosting CD8+ T-cell responses [67]. Similarly, the inhibitory checkpoint receptor TIGIT, which shares the same ligand as CD96, exhibits a comparable phenotype. Combining anti-TIGIT with anti-PD-1 therapy enhances CD8+ T-cell responses and reduces MDSCs *in vivo* [68]. Therefore, identifying suitable ICIs to enhance the immune response, in combination with MAP17 inhibitors, could provide a therapeutic strategy to target the crosstalk between GSCs and immunosuppressive cells.

In addition to immune checkpoint modulation for immune evasion, GBM extensively reshapes the immune cellular microenvironment, effectively shutting down the immune response by recruiting various immunosuppressive cells, such as MDSCs and tumor-associated macrophages (TAMs). It is interesting to acknowledge the additional role of macrophages in GBM in promoting the transition to mesenchymal-like phenotypes, contributing to tumor aggressiveness [69]. This delicate balance between secretory mediators and the immune environment underscores the complexity of the GBM microenvironment and highlights the potential role of MAP17 in modulating these immune dynamics. To explore immune-GBM crosstalk, *MAP17*-overexpressing GBM or GSC lines can be co-cultured with immune cells, such as macrophages or cytotoxic T cells, in a 3D organoid system. Single cell RNA-sequencing can then assess transcriptomic reprogramming in both GSCs and immune cells during co-culture. Additionally, *MAP17*-overexpressing, or knockdown GBM cells can be injected into immunocompromised mice to study MAP17-associated cellular composition and therapeutic responses to ICIs. Experimental approaches such as *in vivo* imaging, flow cytometry, immunofluorescence, and ELISA will provide insights into tumor growth, immune checkpoint expression, infiltrating immune cells, and cytokine secretion, elucidating MAP17's role in the immune microenvironment and GBM dynamics.

It is important to acknowledge several limitations in the present study. First, the predictive association between *MAP17* and GBM is primarily based on public datasets. Second, the study is constrained by the retrospective na-

ture of TCGA data, which may not fully capture the variability and heterogeneity present in patient populations. While our bioinformatics analyses offer valuable insights into *MAP17*'s association with SCCs in GBM, the complementary *in vitro* and *in vivo* experimental studies are crucial to validate the bioinformatic findings in our research to ensure the conclusions. For example, experimental validation such as proteomic, metabolomic, and spatial transcriptomics will be able to validate the protein expression across patients, the metabolic profiles, and the localization of MAP17 positive cells within tumor tissue. These approaches will confirm the observed correlations and elucidate the underlying mechanisms of MAP17 in GBM tumorigenesis. The multimodal approaches in combining multiple modalities which integrate omics with biomedical and clinical information, can also provide valuable insights into the clinical relevance of the biomarker predictions [70].

Conclusion

In conclusion, our bioinformatic analysis suggest that *MAP17* can be a promising biomarker associated with slow-cycling clones in GBM, exhibiting several aggressive features such as mesenchymal phenotype, stemness characteristics, and an immunosuppressive microenvironment in GBM. Future research should focus on evaluating the potential of combinatorial drug approaches, including ICIs, vaccine therapy, metabolic inhibitors, and cell-based therapies, alongside MAP17 inhibitors. These studies, conducted both *in vitro* and *in vivo*, will be crucial for assessing the effectiveness of targeting MAP17 to precisely eliminate therapy-resistant subclones within the GBM tumor.

Availability of Data and Materials

The analyzed data sets generated during the study are available from the corresponding author on reasonable request.

Author Contributions

SSA corrected, revised, provided critical feedback, contributed ideas, and finalized the manuscript. RA conceived the original idea, wrote, revised, and supplemented the manuscript. Both authors were involved in the drafting and critical revision of the manuscript. Both authors have read and approved the final manuscript. Both authors have participated sufficiently in the work and agreed to be accountable for all aspects of the work.

Ethics Approval and Consent to Participate

Not applicable.

Acknowledgment

Not applicable.

Funding

This research received no external funding.

Conflict of Interest

Rada Amin is serving as one of the Guest editors of this journal. We declare that Rada Amin had no involvement in the review of this article and has no access to information regarding its review. The authors declare no conflict of interest.

Supplementary Material

Supplementary material associated with this article can be found, in the online version, at https://doi.org/10.24976/Discov.Med.202537192.14.

References

[1] Mathur R, Wang Q, Schupp PG, Nikolic A, Hilz S, Hong C, *et al*. Glioblastoma evolution and heterogeneity from a 3D whole-tumor perspective. Cell. 2024; 187: 446–463.e16.

[2] Prager BC, Bhargava S, Mahadev V, Hubert CG, Rich JN. Glioblastoma Stem Cells: Driving Resilience through Chaos. Trends in Cancer. 2020; 6: 223–235.

[3] Yalamarty SSK, Filipczak N, Li X, Subhan MA, Parveen F, Ataide JA, *et al*. Mechanisms of Resistance and Current Treatment Options for Glioblastoma Multiforme (GBM). Cancers. 2023; 15: 2116.

[4] Xu C, Hou P, Li X, Xiao M, Zhang Z, Li Z, *et al*. Comprehensive understanding of glioblastoma molecular phenotypes: classification, characteristics, and transition. Cancer Biology & Medicine. 2024; 21: 363–381.

[5] Yang C, Tian G, Dajac M, Doty A, Wang S, Lee JH, *et al*. Slow-Cycling Cells in Glioblastoma: A Specific Population in the Cellular Mosaic of Cancer Stem Cells. Cancers. 2022; 14: 1126.

[6] Chen J, Li Y, Yu TS, McKay RM, Burns DK, Kernie SG, *et al*. A restricted cell population propagates glioblastoma growth after chemotherapy. Nature. 2012; 488: 522–526.

[7] Hassn Mesrati M, Behrooz AB, Y Abuhamad A, Syahir A. Understanding Glioblastoma Biomarkers: Knocking a Mountain with a Hammer. Cells. 2020; 9: 1236.

[8] Rodriguez SMB, Staicu GA, Sevastre AS, Baloi C, Ciubotaru V, Dricu A, *et al*. Glioblastoma Stem Cells-Useful Tools in the Battle against Cancer. International Journal of Molecular Sciences. 2022; 23: 4602.

[9] Aghamiri SS, Amin R. Cancer stem cell metastatic checkpoints and glycosylation patterns: implications for therapeutic strategies. Kinases and Phosphatases. 2024; 2: 151–165.

[10] Tataranu LG, Turliuc S, Rizea RE, Dricu A, Alexandru O, Staicu GA, *et al*. A Synopsis of Biomarkers in Glioblastoma: Past and Present. Current Issues in Molecular Biology. 2024; 46: 6903–6939.

[11] Lin H, Liu C, Hu A, Zhang D, Yang H, Mao Y. Understanding the immunosuppressive microenvironment of glioma: mechanistic insights and clinical perspectives. Journal of Hematology & Oncology. 2024; 17: 31.

[12] Pearson JRD, Cuzzubbo S, McArthur S, Durrant LG, Adhikaree

J, Tinsley CJ, *et al*. Immune Escape in Glioblastoma Multiforme and the Adaptation of Immunotherapies for Treatment. Frontiers in Immunology. 2020; 11: 582106.

[13] Khot S, Krishnaveni A, Gharat S, Momin M, Bhavsar C, Omri A. Innovative drug delivery strategies for targeting glioblastoma: overcoming the challenges of the tumor microenvironment. Expert Opinion on Drug Delivery. 2024; 21: 1837–1857.

[14] Schalper KA, Rodriguez-Ruiz ME, Diez-Valle R, López-Janeiro A, Porciuncula A, Idoate MA, *et al*. Neoadjuvant nivolumab modifies the tumor immune microenvironment in resectable glioblastoma. Nature Medicine. 2019; 25: 470–476.

[15] Zeng YF, Wei XY, Guo QH, Chen SY, Deng S, Liu ZZ, *et al*. The efficacy and safety of anti-PD-1/PD-L1 in treatment of glioma: a single-arm meta-analysis. Frontiers in Immunology. 2023; 14: 1168244.

[16] Wang H, Yang J, Li X, Zhao H. Current state of immune checkpoints therapy for glioblastoma. Heliyon. 2024; 10: e24729.

[17] Goldman MJ, Craft B, Hastie M, Repečka K, McDade F, Kamath A, *et al*. Visualizing and interpreting cancer genomics data via the Xena platform. Nature Biotechnology. 2020; 38: 675–678.

[18] Min M, Spencer SL. Spontaneously slow-cycling subpopulations of human cells originate from activation of stress-response pathways. PLoS Biology. 2019; 17: e3000178.

[19] Aulestia FJ, Néant I, Dong J, Haiech J, Kilhoffer MC, Moreau M, *et al*. Quiescence status of glioblastoma stem-like cells involves remodelling of Ca^{2+} signalling and mitochondrial shape. Scientific Reports. 2018; 8: 9731.

[20] Wang Z, Zhang H, Xu S, Liu Z, Cheng Q. The adaptive transition of glioblastoma stem cells and its implications on treatments. Signal Transduction and Targeted Therapy. 2021; 6: 124.

[21] Tang Z, Li C, Kang B, Gao G, Li C, Zhang Z. GEPIA: a web server for cancer and normal gene expression profiling and interactive analyses. Nucleic Acids Research. 2017; 45: W98–W102.

[22] Li T, Fu J, Zeng Z, Cohen D, Li J, Chen Q, *et al*. TIMER2.0 for analysis of tumor-infiltrating immune cells. Nucleic Acids Research. 2020; 48: W509–W514.

[23] Ru B, Wong CN, Tong Y, Zhong JY, Zhong SSW, Wu WC, *et al*. TISIDB: an integrated repository portal for tumor-immune system interactions. Bioinformatics (Oxford, England). 2019; 35: 4200–4202.

[24] Szklarczyk D, Gable AL, Lyon D, Junge A, Wyder S, Huerta-Cepas J, *et al*. STRING v11: protein-protein association networks with increased coverage, supporting functional discovery in genome-wide experimental datasets. Nucleic Acids Research. 2019; 47: D607–D613.

[25] Liu L, Yang Y, Duan H, He J, Sun L, Hu W, *et al*. CHI3L2 Is a Novel Prognostic Biomarker and Correlated With Immune Infiltrates in Gliomas. Frontiers in Oncology. 2021; 11: 611038.

[26] Kałuzińska-Kołat Ż, Kołat D, Kośla K, Płuciennik E, Bednarek AK. Delineating the glioblastoma stemness by genes involved in cytoskeletal rearrangements and metabolic alterations. World Journal of Stem Cells. 2023; 15: 302–322.

[27] Zhang H, Xu Y, Deng G, Yuan F, Tan Y, Gao L, *et al*. SAA1 knockdown promotes the apoptosis of glioblastoma cells via downregulation of AKT signaling. Journal of Cancer. 2021; 12: 2756–2767.

[28] Yu W, Zhou M, Niu H, Li J, Li Q, Xu X, *et al*. Prognostic marker CXCL5 in glioblastoma polyformis and its mechanism of immune invasion. BMC Cancer. 2024; 24: 140.

[29] Sawai CM, Babovic S, Upadhaya S, Knapp DJHF, Lavin Y, Lau CM, *et al*. Hematopoietic Stem Cells Are the Major Source of Multilineage Hematopoiesis in Adult Animals. Immunity. 2016; 45: 597–609.

[30] Zhu J, Wang H, Ji X, Zhu L, Sun Q, Cong Z, *et al*. Differential Nrf2 expression between glioma stem cells and non-stem-like cells in glioblastoma. Oncology Letters. 2014; 7: 693–698.

[31] Nakada M, Nambu E, Furuyama N, Yoshida Y, Takino T, Hayashi Y, *et al*. Integrin $\alpha 3$ is overexpressed in glioma stem-like cells and promotes invasion. British Journal of Cancer. 2013; 108: 2516–2524.

[32] Richardson PJ. CXCR4 and Glioblastoma. Anti-cancer Agents in Medicinal Chemistry. 2016; 16: 59–74.

[33] Gilder AS, Natali L, Van Dyk DM, Zalfa C, Banki MA, Pizzo DP, *et al*. The Urokinase Receptor Induces a Mesenchymal Gene Expression Signature in Glioblastoma Cells and Promotes Tumor Cell Survival in Neurospheres. Scientific Reports. 2018; 8: 2982.

[34] Patrick S, Lathoria K, Suri V, Sen E. Reduced YAP1 and FOLR1 in gliomas predict better response to chemotherapeutics. Cellular Signalling. 2023; 109: 110738.

[35] Nawaz FZ, Kipreos ET. Emerging roles for folate receptor FOLR1 in signaling and cancer. Trends in Endocrinology and Metabolism: TEM. 2022; 33: 159–174.

[36] Cheng J, Fan YQ, Liu BH, Zhou H, Wang JM, Chen QX. ACSL4 suppresses glioma cells proliferation via activating ferroptosis. Oncology Reports. 2020; 43: 147–158.

[37] Mashima T, Sato S, Sugimoto Y, Tsuruo T, Seimiya H. Promotion of glioma cell survival by acyl-CoA synthetase 5 under extracellular acidosis conditions. Oncogene. 2009; 28: 9–19.

[38] Castro F, Cardoso AP, Gonçalves RM, Serre K, Oliveira MJ. Interferon-Gamma at the Crossroads of Tumor Immune Surveillance or Evasion. Frontiers in Immunology. 2018; 9: 847.

[39] Pribanic S, Gisler SM, Bacic D, Madjdpour C, Hernando N, Sorribas V, *et al*. Interactions of MAP17 with the NaPi-IIa/PDZK1 protein complex in renal proximal tubular cells. American Journal of Physiology. Renal Physiology. 2003; 285: F784–F791.

[40] Kocher O, Cheresh P, Lee SW. Identification and partial characterization of a novel membrane-associated protein (MAP17) upregulated in human carcinomas and modulating cell replication and tumor growth. The American Journal of Pathology. 1996; 149: 493–500.

[41] García-Heredia JM, Carnero A. Dr. Jekyll and Mr. Hyde: MAP17's up-regulation, a crosspoint in cancer and inflammatory diseases. Molecular Cancer. 2018; 17: 80.

[42] Carnero A. MAP17 and the double-edged sword of ROS. Biochimica et Biophysica Acta. 2012; 1826: 44–52.

[43] García-Heredia JM, Otero-Albiol D, Pérez M, Pérez-Castejón E, Muñoz-Galván S, Carnero A. Breast tumor cells promotes the horizontal propagation of EMT, stemness, and metastasis by transferring the MAP17 protein between subsets of neoplastic cells. Oncogenesis. 2020; 9: 96.

[44] Zhang W, Zheng D, Jin L, Hirachan S, Bhandari A, Li Y, *et al*. PDZK1IP1 gene promotes proliferation, migration, and invasion in papillary thyroid carcinoma. Pathology, Research and Practice. 2022; 238: 154091.

[45] Dong F, Li R, Wang J, Zhang Y, Yao J, Jiang SH, *et al*. Hypoxia-dependent expression of MAP17 coordinates the Warburg effect to tumor growth in hepatocellular carcinoma. Journal of Experimental & Clinical Cancer Research: CR. 2021; 40: 121.

[46] Garcia-Heredia JM, Lucena-Cacace A, Verdugo-Sivianes EM, Pérez M, Carnero A. The Cargo Protein MAP17 (PDZK1IP1) Regulates the Cancer Stem Cell Pool Activating the Notch Pathway by Abducting NUMB. Clinical Cancer Research: an Official Journal of the American Association for Cancer Research. 2017; 23: 3871–3883.

[47] Shao Y, Lv H, Zhong DS, Zhou QH. EGFR-TKI resistance and MAP17 are associated with cancer stem cell like properties. Oncology Letters. 2018; 15: 6655–6665.

[48] Su YH, Huang WC, Huang TH, Huang YJ, Sue YK, Huynh TT, *et al*. Folate deficient tumor microenvironment promotes epithelial-to-mesenchymal transition and cancer stem-like phenotypes. Oncotarget. 2016; 7: 33246–33256.

[49] Zgheib R, Battaglia-Hsu SF, Hergalant S, Quéré M, Alberto JM, Chéry C, *et al*. Folate can promote the methionine-dependent reprogramming of glioblastoma cells towards pluripotency. Cell Death & Disease. 2019; 10: 596.

[50] Okada M, Suzuki S, Togashi K, Sugai A, Yamamoto M, Kitanaka C. Targeting Folate Metabolism Is Selectively Cytotoxic to Glioma Stem Cells and Effectively Cooperates with Differentiation Therapy to Eliminate Tumor-Initiating Cells in Glioma Xenografts. International Journal of Molecular Sciences. 2021; 22: 11633.

[51] Ninsontia C, Phiboonchaiyanan PP, Kiratipaiboon C, Chanvorachote P. Zinc suppresses stem cell properties of lung cancer cells through protein kinase C-mediated β-catenin degradation. American Journal of Physiology. Cell Physiology. 2017; 312: C487–C499.

[52] Sahibdad I, Khalid S, Chaudhry GR, Salim A, Begum S, Khan I. Zinc enhances the cell adhesion, migration, and self-renewal potential of human umbilical cord derived mesenchymal stem cells. World Journal of Stem Cells. 2023; 15: 751–767.

[53] Mao P, Joshi K, Li J, Kim SH, Li P, Santana-Santos L, *et al*. Mesenchymal glioma stem cells are maintained by activated glycolytic metabolism involving aldehyde dehydrogenase 1A3. Proceedings of the National Academy of Sciences of the United States of America. 2013; 110: 8644–8649.

[54] Rivero M, Peinado-Serrano J, Muñoz-Galvan S, Espinosa-Sánchez A, Suarez-Martinez E, Felipe-Abrio B, *et al*. MAP17 (PDZK1IP1) and pH2AX are potential predictive biomarkers for rectal cancer treatment efficacy. Oncotarget. 2018; 9: 32958–32971.

[55] Perez M, García-Heredia JM, Felipe-Abrio B, Muñoz-Galván S, Martín-Broto J, Carnero A. Sarcoma stratification by combined pH2AX and MAP17 (PDZK1IP1) levels for a better outcome on doxorubicin plus olaparib treatment. Signal Transduction and Targeted Therapy. 2020; 5: 195.

[56] Muñoz-Galván S, Gutierrez G, Perez M, Carnero A. MAP17 (PDZKIP1) Expression Determines Sensitivity to the Proteasomal Inhibitor Bortezomib by Preventing Cytoprotective Autophagy and NFκB Activation in Breast Cancer. Molecular Cancer Therapeutics. 2015; 14: 1454–1465.

[57] Ferrer I, Quintanal-Villalonga Á, Molina-Pinelo S, Garcia-Heredia JM, Perez M, Suárez R, *et al*. MAP17 predicts sensitivity to platinum-based therapy, EGFR inhibitors and the proteasome inhibitor bortezomib in lung adenocarcinoma. Journal of Experimental & Clinical Cancer Research: CR. 2018; 37: 195.

[58] García-Heredia JM, Carnero A. The cargo protein MAP17 (PDZK1IP1) regulates the immune microenvironment. Oncotarget. 2017; 8: 98580–98597.

[59] Al-Kharboosh R, ReFaey K, Lara-Velazquez M, Grewal SS, Imitola J, Quiñones-Hinojosa A. Inflammatory Mediators in Glioma Microenvironment Play a Dual Role in Gliomagenesis and Mesenchymal Stem Cell Homing: Implication for Cellular Therapy. Mayo Clinic Proceedings. Innovations, Quality & Outcomes. 2020; 4: 443–459.

[60] Yang W, Li Y, Gao R, Xiu Z, Sun T. MHC class I dysfunction of glioma stem cells escapes from CTL-mediated immune response via activation of Wnt/β-catenin signaling pathway. Oncogene. 2020; 39: 1098–1111.

[61] Noh M, Yeo H, Ko J, Kim HK, Lee CH. MAP17 is associated with the T-helper cell cytokine-induced down-regulation of filaggrin transcription in human keratinocytes. Experimental Dermatology. 2010; 19: 355–362.

[62] Arrieta VA, Dmello C, McGrail DJ, Brat DJ, Lee-Chang C, Heimberger AB, *et al*. Immune checkpoint blockade in glioblastoma: from tumor heterogeneity to personalized treatment. The Journal of Clinical Investigation. 2023; 133: e163447.

[63] Guo Q, Shen S, Guan G, Zhu C, Zou C, Cao J, *et al*. Cancer cell intrinsic TIM-3 induces glioblastoma progression. iScience. 2022; 25: 105329.

[64] Curigliano G, Gelderblom H, Mach N, Doi T, Tai D, Forde PM, *et al*. Phase I/Ib Clinical Trial of Sabatolimab, an Anti-TIM-3 Antibody, Alone and in Combination with Spartalizumab, an Anti-PD-1 Antibody, in Advanced Solid Tumors. Clinical Cancer Research: an Official Journal of the American Association for Cancer Research. 2021; 27: 3620–3629.

[65] Zhang Q, Zhong H, Fan Y, Liu Q, Song J, Yao S, *et al*. Immune and Clinical Features of *CD96* Expression in Glioma by *in silico* Analysis. Frontiers in Bioengineering and Biotechnology. 2020; 8: 592.

[66] Liu F, Huang J, He F, Ma X, Fan F, Meng M, *et al*. CD96, a new immune checkpoint, correlates with immune profile and clinical outcome of glioma. Scientific Reports. 2020; 10: 10768.

[67] Wang Y, Wang C, Qiu J, Qu X, Peng J, Lu C, *et al*. Targeting CD96 overcomes PD-1 blockade resistance by enhancing CD8+ TIL function in cervical cancer. Journal for Immunotherapy of Cancer. 2022; 10: e003667.

[68] Raphael I, Kumar R, McCarl LH, Shoger K, Wang L, Sandlesh P, *et al*. TIGIT and PD-1 Immune Checkpoint Pathways Are Associated With Patient Outcome and Anti-Tumor Immunity in Glioblastoma. Frontiers in Immunology. 2021; 12: 637146.

[69] Hara T, Chanoch-Myers R, Mathewson ND, Myskiw C, Atta L, Bussema L, *et al*. Interactions between cancer cells and immune cells drive transitions to mesenchymal-like states in glioblastoma. Cancer Cell. 2021; 39: 779–792.e11.

[70] Isavand P, Aghamiri SS, Amin R. Applications of Multimodal Artificial Intelligence in Non-Hodgkin Lymphoma B Cells. Biomedicines. 2024; 12: 1753.